Istanbul Bridge Conference
August 11-13, 2014
Istanbul, Turkey

SPATIAL EMBEDDED SLIP MODEL FOR ANALYZING COUPLING TIME-RELATIVE EFFECTS OF CREEP AND PRESTRESS OF PC BRIDGES

Cheng Ma[1] and Wei-zhen Chen[2]

ABSTRACT

A spatial embedded slip model is presented in this paper for analyzing the coupling time-relative effect of creep and prestress of prestressed concrete (PC) bridges. This model is made up of three components: a three-dimensional (3D) solid element that describes the behavior of concrete, a truss element that describes the behavior of tendon, and a non-thickness bond element that describes the interface of tendon and concrete. The bond element is embedded into the slip model through virtual nodes set on the intersection points of tendon and concrete. Also established in this paper is an elastic finite element equilibrium equation based on displacement-based finite element framework and constitutive relation of each component. Besides, the creep coefficient in prevailing Chinese Bridge Design Code is fitted using quasi-linear regression method, on the basis of which a finite element equilibrium equation for analyzing coupling time-relative effects of creep and prestress is then derived. The proposed model allows tendon to go through concrete in any patterns, accounting for factors such as concrete aging differences. Correlation studies are conducted upon a series of prestressed concrete beams, using the slip model, and accuracy of it is fully verified.

[1]Ph.D Student, Dept. of Bridge Engineering, Univ. of Tongji, Shanghai, 200092
[2]Professor, Dept. of Civil Engineering, Univ. of Tongji, Shanghai, 200092

Cheng Ma, Wei-zhen Chen. Spatial embedded slip model for analyzing coupling time-relative effects of creep and prestress of PC bridges. *Proceedings of the Istanbul Bridge Conference*, 2014.

Spatial Embedded Slip Model for Analyzing Coupling Time-relative Effects of Creep and Prestress of PC Bridges

Cheng Ma[1] and Wei-zhen Chen[2]

ABSTRACT

A spatial embedded slip model is presented in this paper for analyzing the coupling time-relative effect of creep and prestress of prestressed concrete (PC) bridges. This model is made up of three components: a three-dimensional (3D) solid element that describes the behavior of concrete, a truss element that describes the behavior of tendon, and a non-thickness bond element that describes the interface of tendon and concrete. The bond element is embedded into the slip model through virtual nodes set on the intersection points of tendon and concrete. Also established in this paper is an elastic finite element equilibrium equation based on displacement-based finite element framework and constitutive relation of each component. Besides, the creep coefficient in prevailing Chinese Bridge Design Code is fitted using quasi-linear regression method, on the basis of which a finite element equilibrium equation for analyzing coupling time-relative effects of creep and prestress is then derived. The proposed model allows tendon to go through concrete in any patterns, accounting for factors such as concrete aging differences. Correlation studies are conducted upon a series of prestressed concrete beams, using the slip model, and accuracy of it is fully verified.

Introduction

Prestressed concrete (PC) bridges are popularly chosen in practical engineering for their advantages in construction and service over other bridge types. The simulation methods of concrete and tendon, the two main materials for bridges, are of great importance to the numerical study. Currently, most of the design calculation of the bridges is based on the beam-based finite element model, where the plane-section assumption is required and the prestress is treated as equivalent force acted on the member [1]. The beam-based model has a high efficiency in calculation while its drawbacks are obvious at the same time. For example, it ignores the tendon slip, neglects the impact of concrete deformation on prestressing force, and lacks ability both in reflecting the spatial mechanic state of the structure and calculating the prestress loss accurately. In order to solve these problems, various kinds of entity finite element models are introduced to the advanced analysis of PC bridges, in which the tendon is modeled as independent element, contributing to the overall stiffness and load of the structure. There are mainly two approaches [2] for these entity models in dealing with the interaction between concrete and tendon, the embedded model and the separated model. The traditional embedded model, where tendon is regarded to be fully bonded with concrete, provides convenience in finite element mesh but misses the consideration of tendon slip. The separated model, which can simulate the behavior of the interface of concrete and tendon through bond element, usually, however, needs tendon located at the boundary of concrete. When tendon layout is complicated, the preprocessing work would be inevitably troublesome. At present, a series of tendon models (e.g., Kang [3]; Van Zyl and Scordelis [4]; Van Greunen and

[1]Ph.D Student, Dept. of Bridge Engineering, Univ. of Tongji, Shanghai, 200092
[2]Professor, Dept. of Bridge Engineering, Univ. of Tongji, Shanghai, 200092

Cheng Ma, Wei-zhen Chen. Spatial embedded slip model for analyzing coupling time-relative effects of creep and prestress of PC bridges. *Proceedings of the Istanbul Bridge Conference*, 2014.

Scordelis [5]; Mari [6]; Roca and Mari [7]; Cruz et al. [8]; Wu et al. [9]) have been proposed for PC structures, but most of them are considered within the 2D space with concrete modeled by plane element or shell element.

In addition, the creep effect, as an important time-dependent property of concrete, also has a strong influence on the structure. The accurate consideration of the creep effect relies on several aspects, such as the calculation of the creep coefficient and the storage of concrete stress. Zienkiewiz et al. [10], on taking advantage of the characteristics of exponential function, provided an explicit solution of equal step for creep analysis. The solution was improved by Zhu [11], who provided an explicit solution as well as an implicit solution of variable step. Meanwhile, the aging difference of concrete is in need of attention since concrete creep has a strong sensitivity to time.

In this study, a spatial embedded slip model which incorporates the advantages of the traditional embedded and separated model is presented to analyze the time-relative coupling effects of creep and prestress upon PC bridges. The finite element equilibrium equation of the model is established within the displacement-based finite element framework to well consider the displacement modes and material constitutive relations of its components. Furthermore, the incremental equation for creep analysis is inserted into the equilibrium equation as well as considering the aging differences. A corresponding program is developed using fortran language and a modified Newton-Raphson iteration algorithm is adopted so that the stiffness and load matrix of the model can be automatically updated within the solution.

Spatial embedded slip model

The spatial embedded slip model is made up of three components: (1) a 20-node 3D solid element for simulation of concrete; (2) a 2-node truss element for simulation of tendon; and (3) a 4-node non-thickness bond element for simulation of the interface of the two. At the same time, three coordinate systems are adopted, such as *oxyz* for the global coordinate system, $o'\xi\eta\zeta$ for the local coordinate system of the concrete element, and $o_1tr_1r_2$ for the local coordinate system shared by the tendon element and the bond element. It is appointed that the corner marks of cor1, cor2, and cor3 in the equations of this paper are meant to refer to *oxyz*, $o'\xi\eta\zeta$, and $o_1tr_1r_2$, respectively. Shown in Fig. 1 is the discrete form of the spatial embedded slip model, where 1~20 are the nodes of the concrete element, *i* and *j* are the nodes of the tendon element, *m* and *n* are the virtual nodes [12] set at the intersection points of these two. At the initial moment, *m* and *n* should coincide with *i* and *j*, respectively. It is regarded that tendon is fully bonded with concrete in radial directions. As shown in Fig. 1, the internal and the external surface of the bond element share common nodes of *i* and *j* as well as common virtual nodes of *m* and *n* with, respectively, the tendon element and the concrete element.

The vector of tendon slippage in the local coordinate system of $o_1tr_1r_2$ is

$$\{s\} = \{u\}^{A}_{\text{cor3}} - \{u\}^{A'}_{\text{cor3}} = \begin{bmatrix} s_t & s_{r1} & s_{r2} \end{bmatrix}^{\mathrm{T}} \tag{1}$$

where *A* and *A*' respectively corresponds to the point on the external and internal surface of the bond element at local tangential coordinate *t* ($-1 \le t \le 1$); s_t=tangential tendon slippage; s_{r1} and s_{r2}=relative displacement of tendon and concrete in the direction of o_1r_1 and o_1r_2, respectively.

The displacements of point *A* and *A*' in the global coordinate system of *oxyz* are

$$\{u\}^{A}_{\text{cor1}} = [N]_{\text{s}}\{u\}^{mn} \tag{2}$$

$$\{u\}^{A'}_{\text{cor1}} = [N]_{\text{s}}\{u\}_{\text{s}} \tag{3}$$

where $\{u\}^{mn} = [u_x^m \quad u_y^m \quad u_z^m \quad u_x^n \quad u_y^n \quad u_z^n]^{\mathrm{T}}$ =vector of displacements of nodes *m* and *n*; $\{u\}_{\text{s}} = [u_x^i \quad u_y^i \quad u_z^i \quad u_x^j \quad u_y^j \quad u_z^j]^{\mathrm{T}}$ =vector of nodal displacements of tendon;

$[N]_s = \left[(1-t)[I]/2 \quad (1+t)[I]/2\right]$=shape function matrix of tendon, with [*I*]=3×3 unit matrix.

Let $\{u\}_c=[u_x^1 \quad u_y^1 \quad u_z^1 \quad ... \quad u_x^{20} \quad u_y^{20} \quad u_z^{20}]^T$ =vector of nodal displacements of concrete, and $[N]_c$ =shape function matrix of concrete, there is

$$\{u\}^{mn} = [N]_{mn}\{u\}_c \tag{4}$$

where $[N]_{mn}$ =displacement interpolation matrix of nodes *m* and *n*.

Substituting Eq. 4 into Eq. 2 results in

$$\{u\}^A_{cor1} = [N]_s[N]_{mn}\{u\}_c \tag{5}$$

Fig. 2 shows the conversion between the local coordinate system of $o_1tr_1r_2$ and the global coordinate system of *oxyz*. It is noted that φ=angle between axis o_1t and plane *xoy*, θ=angle between axis o_1t' and *ox*, with axis o_1t' the projection of o_1t on plane *xoy*, the displacements of any point in $o_1tr_1r_2$ and *oxyz* satisfy

$$\{u\}_{cor3} = [T]_2[T]_1\{u\}_{cor1} \tag{6}$$

where $[T]_1$ and $[T]_2$ =conversion matrices expressed by θ and φ, respectively.

Combine Eq. 2, 5, and 6 to obtain the vector of slippage expressed by $\{u\}_c$ and $\{u\}_s$

$$\{s\} = [T]_2[T]_1(\{u\}^A_{cor3} - \{u\}^{A'}_{cor3}) = [T]_2[T]_1[N]_s([N]_{mn}\{u\}_c - \{u\}_s) \tag{7}$$

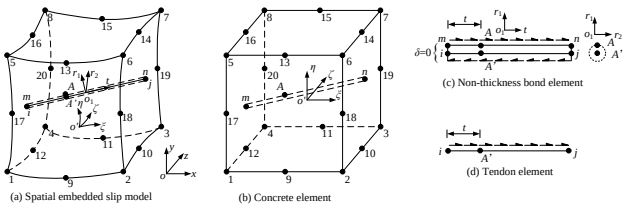

Figure 1. Discrete form of the spatial embedded slip model

Material constitutive relation

In this study, the material constitutive relations of concrete and tendon are considered to be linear elastic, satisfying

$$\{\sigma\}_c = [D]_c\{\varepsilon\}_c = [D]_c[B]_c\{u\}_c \tag{8}$$

$$\{\sigma\}_s = [D]_s\{\varepsilon\}_s = [D]_s[B]_s\{u\}_s \tag{9}$$

where $\{\sigma\}$, $\{\varepsilon\}$, $[D]$, and $[B]$ =matrices of stress, strain, elasticity, and strain transformation, with corner marks of c and s referring to concrete and tendon, respectively.

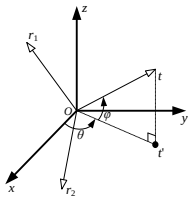

Figure 2. Conversion between local and coordinate systems

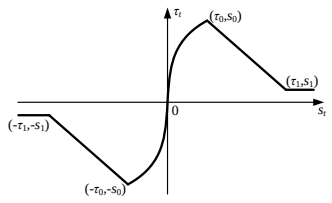

Figure 3. Bond stress-slip curve

As to the bond element, since tendon is assumed to be fully bonded with concrete in its radial directions, a large value which has the same order of magnitude with the elastic modulus of concrete is assigned to the radial stiffness in order to ensure that the radial relative

deformation of concrete and tendon is well coordinated. For the tangential stiffness of the bond element, we choose the bond stress-slip relation proposed by Eligehausen et al. [13], which is shown in Fig. 3, the mathematical equations of the tangential bond stress and stiffness when tendon slippage is larger than zero are

$$\begin{aligned}
&\tau_t = \frac{2\tau_0}{s_0}\left(s_t - \frac{s_t^2}{2s_0}\right),\ k_t = \frac{2\tau_0}{s_0}\left(1-\frac{s_t}{s_0}\right),\ 0 \le s_t \le s_0 \\
&\tau_t = (s_t - s_0)\frac{\tau_1-\tau_0}{s_1-s_0} + \tau_0,\ k_t = \frac{\tau_1-\tau_0}{s_1-s_0},\ s_0 < s_t \le s_1 \\
&\tau_t = \tau_1,\ k_t = 0,\ s_t > s_1
\end{aligned} \tag{10}$$

where τ_t and k_t=tangential bond stress and stiffness, respectively; in this paper, s_0=0.025mm, s_1=20s_0, τ_0=6.64MPa, τ_1=0.2τ_0.

Then the constitutive relation of the bond element is

$$\{f\}_{\mathrm{b}} = [k]_{\mathrm{b}}\{s\} = [k]_{\mathrm{b}}[T]_2[T]_1[N]_{\mathrm{s}}([N]_{mn}\{u\}_{\mathrm{c}} - \{u\}_{\mathrm{s}}) \tag{11}$$

where $\{f\}_{\mathrm{b}} = \begin{bmatrix}\tau_t & \sigma_{r1} & \sigma_{r2}\end{bmatrix}^{\mathrm{T}}$=vector of force per unit area for the bond element, with σ_{r1} and σ_{r2}=orthogonal radial bond stresses; $\boldsymbol{k}_{\mathrm{b}} = \begin{bmatrix} k_t & & \\ & k_{r1} & \\ & & k_{r2}\end{bmatrix}$=stiffness matrix of the bond element corresponding to the local coordinate system of $o_1tr_1r_2$, with k_{r1} and k_{r2}=orthogonal radial stiffness in the directions of o_1r_1 and o_1r_2, respectively.

Equilibrium equation of the slip model

With the solution found at step *i*, where the stress and force vectors of concrete, tendon and the bond element are denoted as $\{\sigma\}_{\mathrm{c},i}$, $\{\sigma\}_{\mathrm{s},i}$, and $\{f\}_{\mathrm{b},i}$, respectively, equilibrating external force vectors $\{P\}_{\mathrm{c},i}$ and $\{P\}_{\mathrm{s},i}$ applied on the nodes of concrete and tendon, the incremental form of the virtual work principle can be used to obtain the solution at step $i+\Delta i$

$$\begin{aligned}
&\int_{V_{\mathrm{c}}}([B]_{\mathrm{c}}\delta\{\Delta u\}_{\mathrm{c},i})^{\mathrm{T}}(\{\sigma\}_{\mathrm{c},i}+\{\Delta\sigma\}_{\mathrm{c},i})dV_{\mathrm{c}} + A_{\mathrm{s}}\int_{\Gamma_{\mathrm{s}}}([B]_{\mathrm{s}}\delta\{\Delta u\}_{\mathrm{s},i})^{\mathrm{T}}(\{\sigma\}_{\mathrm{s},i}+\{\Delta\boldsymbol{\sigma}\}_{\mathrm{s},i})d\Gamma_{\mathrm{s}} \\
&+C_{\mathrm{s}}\int_{\Gamma_{\mathrm{b}}}(\delta\{\Delta s\}_{\mathrm{b},i})^{\mathrm{T}}(\{f\}_{\mathrm{b},i}+\{\Delta f\}_{\mathrm{b},i})d\Gamma_{\mathrm{b}} = (\delta\{\Delta u\}_{\mathrm{c},i})^{\mathrm{T}}\{P\}_{\mathrm{c},i+\Delta i} + (\delta\{\Delta u\}_{\mathrm{s},i})^{\mathrm{T}}\{P\}_{\mathrm{s},i+\Delta i}
\end{aligned} \tag{12}$$

with V_{c}=concrete volume, Γ_{s} and Γ_{b} =length of tendon and bond element, respectively, A_{s} and C_{s}=area and perimeter of tendon element, and Δ represents the increments.

Substituting Eq. 8, 9, 11 into the three items on the left side of Eq. 12, respectively, there are

$$\delta W_{\mathrm{c,int}} = (\delta\{\Delta u\}_{\mathrm{c},i})^{\mathrm{T}}[R]^{\mathrm{c}}_{\mathrm{cc},i} + (\delta\{\Delta u\}_{\mathrm{c},i})^{\mathrm{T}}[K]^{\mathrm{c}}_{\mathrm{cc}}\{\Delta u\}_{\mathrm{c},i} \tag{13}$$

$$\delta W_{\mathrm{s,int}} = (\delta\{\Delta u\}_{\mathrm{s},i})^{\mathrm{T}}[R]^{\mathrm{s}}_{\mathrm{ss},i} + (\delta\{\Delta u\}_{\mathrm{s},i})^{\mathrm{T}}[K]^{\mathrm{s}}_{\mathrm{ss}}\{\Delta u\}_{\mathrm{s},i} \tag{14}$$

$$\begin{aligned}
\delta W_{\mathrm{b,int}} &= (\delta\{\Delta u\}_{\mathrm{c},i})^{\mathrm{T}}[R]_{\mathrm{bc},i} + (\delta\{\Delta u\}_{\mathrm{s},i})^{\mathrm{T}}[R]_{\mathrm{bs},i} + (\delta\{\Delta u\}_{\mathrm{c},i})^{\mathrm{T}}[K]^{\mathrm{b}}_{\mathrm{cc},i}\{\Delta u\}_{\mathrm{c},i} \\
&\quad + (\delta\{\Delta u\}_{\mathrm{c},i})^{\mathrm{T}}[K]^{\mathrm{b}}_{\mathrm{cs},i}\{\Delta u\}_{\mathrm{s},i} + (\delta\{\Delta u\}_{\mathrm{s},i})^{\mathrm{T}}[K]^{\mathrm{b}}_{\mathrm{sc},i}\{\Delta u\}_{\mathrm{c},i} + (\delta\{\Delta u\}_{\mathrm{s},i})^{\mathrm{T}}[K]^{\mathrm{b}}_{\mathrm{ss},i}\{\Delta u\}_{\mathrm{s},i}
\end{aligned} \tag{15}$$

where $[R]^{\mathrm{c}}_{\mathrm{cc},i} = \int_{V_{\mathrm{c}}}[B]^{\mathrm{T}}_{\mathrm{c}}\{\sigma\}_{\mathrm{c},i}dV_{\mathrm{c}}$; $[R]^{\mathrm{s}}_{\mathrm{ss},i} = A_{\mathrm{s}}\int_{\Gamma_{\mathrm{s}}}[B]^{\mathrm{T}}_{\mathrm{s}}\{\sigma\}_{\mathrm{s},i}d\Gamma_{\mathrm{s}}$;

$[R]^{\mathrm{b}}_{\mathrm{bc},i} = C_{\mathrm{s}}\int_{\Gamma_{\mathrm{b}}}[N]^{\mathrm{T}}_{mn}[N]^{\mathrm{T}}_{\mathrm{s}}[T]^{\mathrm{T}}_1[T]^{\mathrm{T}}_2\{f\}_{\mathrm{b},i}d\Gamma_{\mathrm{b}}$; $[R]^{\mathrm{b}}_{\mathrm{bs},i} = -C_{\mathrm{s}}\int_{\Gamma_{\mathrm{b}}}[N]^{\mathrm{T}}_{\mathrm{s}}[T]^{\mathrm{T}}_1[T]^{\mathrm{T}}_2\{f\}_{\mathrm{b},i}d\Gamma_{\mathrm{b}}$;

$[K]^{\mathrm{c}}_{\mathrm{cc}} = \int_{V_{\mathrm{c}}}[B]^{\mathrm{T}}_{\mathrm{c}}[D]_{\mathrm{c}}[B]_{\mathrm{c}}dV_{\mathrm{c}}$; $[K]^{\mathrm{s}}_{\mathrm{ss}} = A_{\mathrm{s}}\int_{\Gamma_{\mathrm{s}}}[B]^{\mathrm{T}}_{\mathrm{s}}[D]_{\mathrm{s}}[B]_{\mathrm{s}}d\Gamma_{\mathrm{s}}$;

$$[K]^{\mathrm{b}}_{\mathrm{cc},i} = C_{\mathrm{s}}\int_{\Gamma_{\mathrm{b}}} [N]^{\mathrm{T}}_{mn}[N]^{\mathrm{T}}_{\mathrm{s}}[T]^{\mathrm{T}}_{1}[T]^{\mathrm{T}}_{2}[k]_{\mathrm{b},i}[T]_2[T]_1[N]_{\mathrm{s}}[N]_{mn}\,d\Gamma_{\mathrm{b}}\,;$$

$$[K]^{\mathrm{b}}_{\mathrm{cs},i} = -C_{\mathrm{s}}\int_{\Gamma_{\mathrm{b}}} [N]^{\mathrm{T}}_{mn}[N]^{\mathrm{T}}_{\mathrm{s}}[T]^{\mathrm{T}}_{1}[T]^{\mathrm{T}}_{2}[k]_{\mathrm{b},i}[T]_2[T]_1[N]_{\mathrm{s}}\,d\Gamma_{\mathrm{b}}\,;$$

$$[K]^{\mathrm{b}}_{\mathrm{sc},i} = -C_{\mathrm{s}}\int_{\Gamma_{\mathrm{b}}} [N]^{\mathrm{T}}_{\mathrm{s}}[T]^{\mathrm{T}}_{1}[T]^{\mathrm{T}}_{2}[k]_{\mathrm{b},i}[T]_2[T]_1[N]_{\mathrm{s}}[N]_{mn}\,d\Gamma_{\mathrm{b}}\,;$$

$$[K]^{\mathrm{b}}_{\mathrm{ss},i} = C_{\mathrm{s}}\int_{\Gamma_{\mathrm{b}}} [N]^{\mathrm{T}}_{\mathrm{s}}[T]^{\mathrm{T}}_{1}[T]^{\mathrm{T}}_{2}[k]_{\mathrm{b},i}[T]_2[T]_1[N]_{\mathrm{s}}\,d\Gamma_{\mathrm{b}}\,.$$

Substitute Eq. 13, 14, and 15 into Eq. 12, and rewrite it to matrix form to get the basic finite element equilibrium equation of the slip model at step *i*.

$$\begin{bmatrix} [K]^{\mathrm{c}}_{\mathrm{cc}}+[K]^{\mathrm{b}}_{\mathrm{cc},i} & [K]^{\mathrm{b}}_{\mathrm{cs},i} \\ [K]^{\mathrm{b}}_{\mathrm{sc},i} & [K]^{\mathrm{s}}_{\mathrm{ss}}+[K]^{\mathrm{b}}_{\mathrm{ss},i} \end{bmatrix}\begin{bmatrix} \{\Delta u\}_{\mathrm{c},i} \\ \{\Delta u\}_{\mathrm{s},i} \end{bmatrix} = \begin{bmatrix} \{P\}_{\mathrm{c},i+\Delta i} \\ \{P\}_{\mathrm{s},i+\Delta i} \end{bmatrix} - \begin{bmatrix} [R]^{\mathrm{c}}_{\mathrm{cc},i}+[R]^{\mathrm{b}}_{\mathrm{bc},i} \\ [R]^{\mathrm{s}}_{\mathrm{ss},i}+[R]^{\mathrm{b}}_{\mathrm{bs},i} \end{bmatrix} \tag{16}$$

Creep Effect

In this study, the total strain of concrete at age *t* is considered to be the sum of the elastic strain and the creep strain

$$\varepsilon_{\mathrm{c}}(t) = \varepsilon^{\mathrm{e}}_{\mathrm{c}}(t) + \varepsilon^{\mathrm{cr}}_{\mathrm{c}}(t) \tag{17}$$

Shown in Fig. 4 is the time-relative developing curve of the concrete stress, with creep considered from t_0. Noting $\Delta t_n = t_{\mathrm{n}} - t_{n-1}$, $\Delta\sigma_{\mathrm{c},n} = \sigma_{\mathrm{c}}(t_n) - \sigma_{\mathrm{c}}(t_{n-1})$, $\Delta\sigma_{\mathrm{c},0}$=initial concrete stress, E_{c}=elastic modulus of concrete, there are

$$\varepsilon^{\mathrm{e}}_{\mathrm{c}}(t) = \frac{\Delta\sigma_{\mathrm{c},0}}{E_{\mathrm{c}}} + \int_{t_0}^{t}\frac{1}{E_{\mathrm{c}}}\frac{\mathrm{d}\sigma_{\mathrm{c}}}{\mathrm{d}\tau}\,d\tau \tag{18}$$

$$\varepsilon^{\mathrm{cr}}_{\mathrm{c}}(t) = \frac{\Delta\sigma_{\mathrm{c},0}}{E_{\mathrm{c}}}\varphi(t,t_0) + \int_{t_0}^{t}\frac{\varphi(t,\tau)}{E_{\mathrm{c}}}\frac{\mathrm{d}\sigma_{\mathrm{c}}}{\mathrm{d}\tau}\,d\tau \tag{19}$$

where $\varphi(t,\tau)$=creep coefficient; τ=age from the time when creep began. In the current Chinese bridge design code [14], the creep coefficient is defined as

$$\varphi(t,\tau) = \varphi(\tau)\cdot\beta_{\mathrm{c}}(t-\tau) \tag{20}$$

with $\beta_{\mathrm{c}}(t-\tau) = \left[\dfrac{(t-\tau)/t_1}{\beta_{\mathrm{H}}+(t-\tau)/t_1}\right]^{0.3}$ and $\beta_{\mathrm{H}} = 150\left[1+\left(1.2\dfrac{RH}{RH_0}\right)^{18}\right]\dfrac{h}{h_0}+250\le 1500$

where $\varphi(\tau)$=nominal creep coefficient; $\beta_{\mathrm{c}}(t\text{-}\tau)$=development coefficient; β_{H}=coefficient relevant to *RH* and *h*; *RH*=annual average relative humidity; $h=2A/u$=theoretical thickness of component; *A*=cross-sectional area of component; *u*=peripheral length of component in contact with atmosphere; t_1=1d; RH_0=100%; h_0=100mm.

For more convenience in programing, $\beta_{\mathrm{c}}(t\text{-}\tau)$ can be further fitted as

$$\beta_{\mathrm{c}}(t-\tau) = \sum_{j=1}^{3} c_j e^{q_j(t-\tau)} \tag{21}$$

where the values of c_j and q_j (j=1,2,3) are listed in Tab. Shown in Fig. 4 are the fitting and theoretical curves of $\varphi(t,\tau)$ when *RH*=55% and *h*=100*mm*, in which a high accuracy of the fitting equation can be seen.

Combine Eq. 17, 18, 19, and 21 to obtain the creep strain increment within Δt_n

$$\Delta\varepsilon^{\mathrm{cr}}_{\mathrm{c},n} = \varepsilon^{\mathrm{cr}}_{\mathrm{c}}(t_n) - \varepsilon^{\mathrm{cr}}_{\mathrm{c}}(t_{n-1}) = \eta_n + \chi_n\Delta\sigma_{\mathrm{c},n} \tag{22}$$

where $\eta_n = \sum_{j=1}^{3}(e^{q_j\Delta t_n}-1)\omega_{j,n}$, $\chi_n = \dfrac{\varphi(t_n,t_{n-0.5})}{E_{\mathrm{c}}}$,

$$\omega_{j,n}=\omega_{j,n-1}e^{q_j\Delta t_{n-1}}+\frac{\Delta\sigma_{c,n-1}}{E_c}\varphi(t_{n-1-0.5})c_j e^{0.5q_j\Delta t_{n-1}}\text{, with }\omega_{j,1}=\frac{\Delta\sigma_{c,0}}{E_c}\varphi(t_0)c_j\text{.}$$

Table 1. Values of fitting coefficients for $\beta_c(t-\tau)$

RH	*h*/mm	c_1	$q_1(\times10^{-5})$	c_2	$q_2(\times10^{-3})$	c_3	$q_3(\times10^{-2})$
[40%,70%] (*RH*=55%)	100	0.8689	4.5373	-0.4053	-4.4105	-0.4525	-8.4025
	200	0.8346	5.7034	-0.4185	-4.4664	-0.4068	-8.7232
	300	0.8034	6.8497	-0.4146	-3.9733	-0.3788	-8.5285
	600	0.7332	9.2705	-0.3996	-3.6582	-0.3256	-8.6367
	≥833	0.6923	10.654	-0.3805	-3.5026	-0.3036	-8.2968
[70%,99%] (*RH*=80%)	100	0.8523	5.0902	-0.4095	-4.2246	-0.4318	-8.2912
	200	0.8049	6.7806	-0.4167	-3.9919	-0.3799	-8.6855
	300	0.7667	8.1135	-0.4096	-3.7972	-0.3487	-8.6872
	≥600	0.6923	10.654	-0.3805	-3.5026	-0.3063	-8.2968

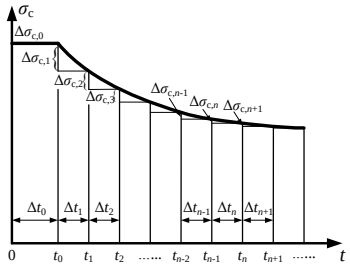

Figure 3. Developing curve of concrete stress

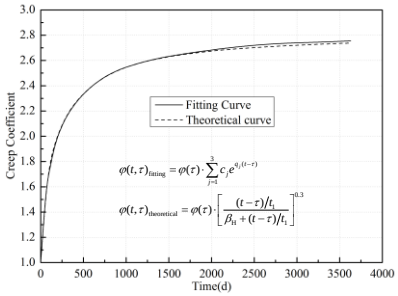

Figure 4. Fitting and theoretical curves of $\varphi(t,\tau)$

A detailed deduction of Eq. 22 can be seen in Cheng Ma [15], where the finite element equilibrium equation for creep analysis of plane concrete within Δt_n is given as

$$[K]^{cr}_{cc,n}\{\Delta u\}_{c,n}=\{\Delta P\}_{c,n}+\{\Delta P\}^{cr}_{c,n} \tag{23}$$

where $[K]^{cr}_{cc,n}=\int_{V_c}[B]^T_c[\overline{D}]_{c,n}[B]_c dV_c$ =creep stiffness matrix of concrete; $[A]=E_c[D]^{-1}_c$; $\{\Delta P\}_{c,n}=\int_{V_c}[B]^T_c\{\Delta\sigma\}_{c,n}dV_c$ and $\{\Delta P\}^{cr}_{c,n}=\int_{V_c}[B]^T_c[\overline{D}]_{c,n}\{\eta\}_n dV_c$ =incremental vectors of external and equivalent forces, respectively; $[\overline{D}]_{c,n}=\frac{1}{1+\chi_n E_c}[D]_c$; $\{\eta\}_n=\sum_{j=1}^{3}(e^{q_j\Delta t_n}-1)\{\omega\}_{j,n}$; $\{\omega\}_{j,n}=e^{q_j\Delta t_{n-1}}\{\omega\}_{j,n-1}+\frac{\varphi(t_{n-1-0.5})c_j e^{0.5q_j\Delta t_{n-1}}}{E_c}[A]\{\Delta\sigma\}_{c,n-1}$, with $\{\omega\}_{j,1}=\frac{\varphi(t_0)c_j}{E_c}[A]\{\Delta\sigma\}_{c,0}$.

The stress of plane concrete satisfies

$$\{\Delta\sigma\}_{c,n}=[\overline{D}]_{c,n}([B]_c\{\Delta u\}_{c,n}-\{\eta\}_n) \tag{24}$$

Substituting Eq. 24 into 12 and replacing step *i* by time step *n*, the finite element equilibrium matrix for creep analysis of the slip model at time step *n* can be obtained

$$\begin{bmatrix}[K]^{cr}_{cc,n}+[K]^{b}_{cc,n} & [K]^{b}_{cs,n}\\ [K]^{b}_{sc,n} & [K]^{s}_{ss}+[K]^{b}_{ss,n}\end{bmatrix}\begin{bmatrix}\{\Delta u\}_{c,n}\\ \{\Delta u\}_{s,n}\end{bmatrix}=\begin{bmatrix}\{P\}_{c,n+\Delta n}+\{\Delta P\}^{cr}_{c,n}\\ \{P\}_{s,n+\Delta n}\end{bmatrix}-\begin{bmatrix}[R]^{c}_{cc,n}+[R]^{\eta}_{cc,n}\\ [R]^{s}_{ss,n}+[R]^{b}_{bs,n}\end{bmatrix} \tag{25}$$

Aging difference

For segmental constructed bridges, the aging difference of each segment should be distinguished and considered as concrete creep has a strong sensitivity to time. In this study, the calculation of each construction stage is divided into two sub-stages of (a) and (b), in which the instant responses and the creep responses of the structure within the constructed stage are calculated, respectively. Shown in Fig. 5 is a two-segment cantilever beam which is denoted as S, with segment ① and ② respectively casted in construction stage 1 and 2. In construction stage 1, the instant responses and creep responses of segment ① are calculated in sub-stage 1(a) and 1(b), respectively, without consideration of aging difference. In construction stage 2, segment ① is treated as an "older" component while segment ② is treated as a "new" one. Therefore, in sub-stage 2(a), only the creep effect should be considered for segment ①, then, as time axis moves to sub-stage 2(b), the concrete in segment ② starts to creep, requiring that the creep effect must be considered both in segment ① and segment ②. It is obvious to see that the aging difference of concrete in segment ① and segment ② equals to the construction time of stage 1. The iterative diagram of the proposed model in considering the aging difference is summarized in Fig. 6.

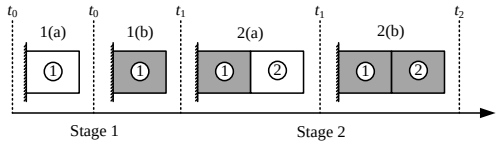

Figure 5. Calculation stages of system S
Note: the segment where concrete creep is in need of consideration is filled with shadow

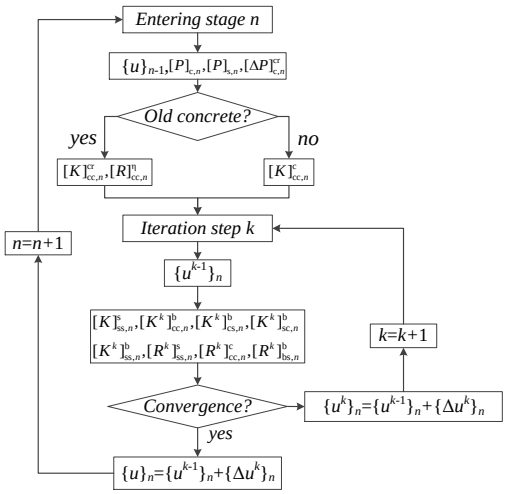

Figure 6. Iterative diagram of the solution

Numerical test

In this chapter, three different beams are considered. The first one (beam I), as seen in Fig. 7, is a plain concrete beam where the creep analysis is conducted. The second one (beam II), as seen in Fig. 8, is a beam chosen from the experiment of Mitchell et al. [16] and was used by Ayoub et al. [17] in his study: for concrete, E_c=3.45×10^{4}MPa, ρ_c=2300kg/m^3; for tendon, E_s=2.049×10^{11}MPa, f_s=1286MPa=tensioning stress, d_s=15.7mm, A_s=146.4mm^2, c=50mm. The third one (beam III), as seen in Fig. 11, is a five-segment cantilever beam of rectangular section, with two tendons in each segment. For concrete, E_c=3.45×10^{4}MPa, ρ_c=2500kg/m^3; for tendon, E_s=2.00×10^{11}MPa, f_s=100MPa, A_s=100mm^2.

Beam I

The creep effect is considered in ten years from t=30d, with time axis divided into six phrases: Δt_1=[31d,41d], Δt_2=[41d,76d], Δt_3=[76d,145d], Δt_4=[145d,365d], Δt_5=[365d,1155d], Δt_6=[1155d,3650d]. For the fitting equation of creep coefficient, c_j and q_j are taken from the

first line of data in Tab. 1. To a determinant plane concrete structure where external forces are applied at one time, the creep coefficient can be derived from the ratio of the creep displacement/strain to the initial elastic displacement/strain. From Tab. 2, it can be seen that the creep coefficient derived either by the calculated displacement or the calculated strain displays a good agreement with the theoretical creep coefficient within each time step, and concrete stress remains steady from beginning to the end, proving that the program has a high accuracy in simulating the creep effect.

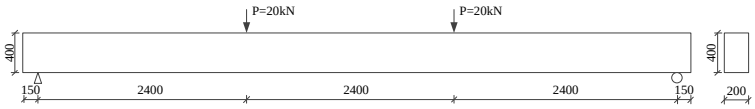

Figure 7. Dimension and load conditions of beam I (Unit: mm)

Table 2. Calculation results of beam I

Step	Age(d)	Mid-span displacement(mm)			Stain($\times10^{-2}$)			Stress(MPa)		Theoretical value of
		T	C	T/E	T	C	T/E	T	C	
Static	31	-14.3	0.0	0.00	-0.051	0.000	0.00	-17.7	0.0	0.00
Step1	41	-25.3	-11.0	0.77	-0.091	-0.040	0.77	-17.7	0.0	0.80
Step2	76	-34.9	-20.6	1.44	-0.126	-0.075	1.47	-17.7	0.0	1.48
Step3	145	-38.9	-24.6	1.72	-0.141	-0.090	1.76	-17.7	0.0	1.76
Step4	365	-45.4	-31.1	2.17	-0.164	-0.113	2.22	-17.7	0.0	2.22
Step5	1155	-50.3	-36.0	2.52	-0.181	-0.130	2.55	-17.7	0.0	2.56
Step6	3650	-54.7	-40.4	2.83	-0.198	-0.147	2.88	-17.7	0.0	2.88

Beam II

In this model, gradation loading proceeds in four steps. Load step 1: tension and anchorage of tendon; Load steps 2~4: concentrated force *P* is applied step by step as per 0→10kN, 10→20kN, and 20→30kN at midspan. For the purpose of comparison, an ANSYS model is established with tendon and concrete respectively simulated by element link 8 and solid 95 in which full bonding is assumed to be existed between the two.

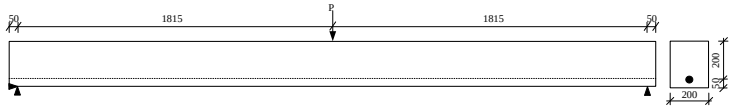

Figure 8. Dimensions and tendon layout of beam II (Unit: mm)

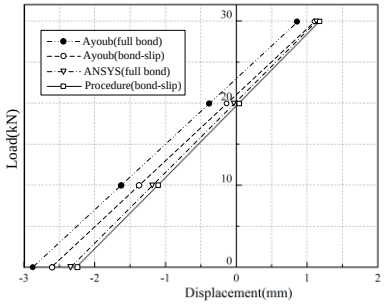

Figure 9. Developing curves of midspan displacements

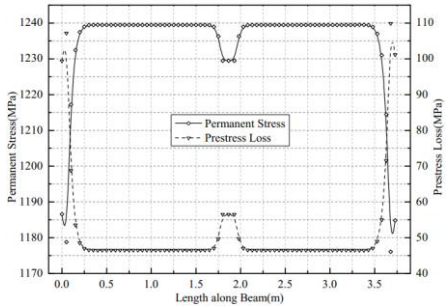

Figure 10. Distribution of permanent stress and prestress loss along the beam after anchorage

The load-displacement responses calculated by the proposed model, ANSYS model and Ayoub's model are shown in Fig. 9. Obviously, the development trends of the four curves are consistent. The load-displacement response obtained by the proposed model draws close to that by ANSYS model, for the element form and the mesh layout of them are the same. Since the proposed model puts tendon slip into consideration, and ANSYS model assumes full bond existing between tendon and concrete, the overall structural stiffness calculated by the proposed model will be smaller than that by ANSYS, and therefore, the midspan displacement calculated by the proposed model will be large than that by ANSYS under the same loading level, which is also provided in Fig.9. Because of the differences in element form, mesh layout and load processing, the calculation result of Ayoub's model is not that close to that of the proposed model although it considers tendon slip. The maximum discrepancy between Ayoub's model and the proposed model reaches as high as 18% at the end of load step 1. Fig. 10 shows the distributions of permanent stress and prestress loss along the beam after anchorage. The prestress loss mounts to the maximum at the end of beam, reaching 105MPa, 8% of the tensioning stress, and attenuates towards midspan, arriving at a stable level of 46MPa. On the contrary, the permanent stress mounts to the maximum t midspan while slacks off at the end of beam, showing a transfer length, as what Ayoub stated in his study.

Beam III

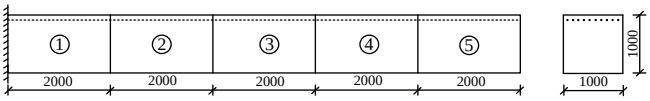

Figure 11. Dimensions and tendon layout of beam III (Unit: mm)

In the process of cantilever construction, the control of the elevation is of great importance to the final bridge line. As shown in Fig.11, although the dimensions of segment ①~⑤ are the same, their stiffness and load contributions to the overall structure are still different for the influence of concrete creep and aging differences. In Fig. 12 is shown the final construct line when segment ⑤ is finished. In the figure, the final displacement of the beam when creep is considered is quite different from that when creep is not considered, indicating that the concrete creep has a significant impact on bridge line of the construction stage. Fig. 13 shows the tendon slippage along the beam. Obviously, the tendon slippage when creep is considered is much larger than that when it is not, explaining that the concrete creep aggravates the interaction between tendon and concrete, and thus further weakens the overall stiffness of the structure.

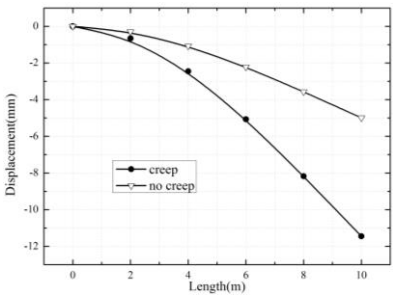

Figure 12. Final displacements of beam III

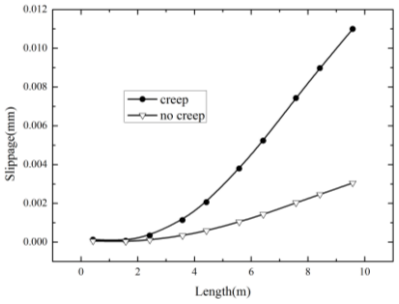

Figure 13. Tendon slippage along the beam

Conclusions

This study presents a spatial slip model for PC bridges, with concrete, tendon and interface of the two simulated by 20-node solid element, 2-node truss element, and 4-node non-thickness bond element, respectively. This model takes tendon slip into consideration with allowing tendon to go through concrete in any patterns, which makes an improvement on the traditional embedded and separated model. The finite element equilibrium equation of the model is deduced and a modified Newton-Raphson iteration algorithm is adopted within the solution of the equilibrium equations so that the stiffness and load matrices of the model can be updated easily. Though numerical studies of three different beams, the accuracy of the slip model is verified, where a distinguish difference between the responses whenever creep effect is considered is easy to see, showing that concrete creep as well as aging difference has a strong impact on the structure.

References

1. Aalami BO. Structural modeling of posttensioned members. *J. Struct. Eng.* 2000; **126**(2): 157-162.
2. Shen JM., Wang CZ, Jiang JJ. *Finite element analysis on reinforced concrete and the ultimate analysis on slab and shell*. Tsinghua University Press, Beijing, 1993.
3. Kang YJ. *Nonlinear geometric, material, and time-dependent analysis of reinforced and prestressed concrete frames*. PhD thesis, University of California, Berkeley, Calif., 1977.
4. Van Zyl SF., Scordelis AC. Analysis of curved, prestressed, segmental bridges. *Journal of the Structural Division* 1979; **105**(11): 2399-2417.
5. Van Greunen J, Scordelis AC. Nonlinear analysis of prestressed concrete slabs. *J. Struct. Eng.* 1983; **109**(7): 1742-1760.
6. Mari AR. *Nonlinear geometric, material and time dependent analysis of three-dimensional reinforced and prestressed concrete frames*. Report. No. 84-12, SESM, University of California, Berkeley, Calif., 1984.
7. Roca P, Mari AR. Nonlinear geometric and material analysis of prestressed concrete general shell structures. *Computers and Structures* 1993; **46**(5): 905-916.
8. Cruz PJS, Mari AR, Roca P. Nonlinear time-dependent analysis of segmentally constructed structures. *J. Struct. Eng.* 1998; **124**(3): 278-287.
9. Wu XH, Otani S, Shiohara H. Tendon model for nonlinear analysis of prestressed concrete structures. *J. Struct. Eng.* 2001; **127**(4): 398-405.
10. Zienkiewicz OC, Watson M, King IP. A numerical method of visco-elastic stress analysis. *International Journal of Mechanical Sciences* 1968; **10**(10): 807-827.
11. Zhu BF. *The finite element method theory and applications*. China Water Power Press, Beijing, 1998.
12. Long YC, Zhang CH, Zhou YD. Embedded slip model for analyzing reinforced concrete structures. *Engineering Mechanics* 2007; **S**(1): 41-43.
13. Eligehausen R, Popov EP, Bertero VV. *Local bond stress-slip relationships of deformed bars under generalized excitations*. Report EERC 83~23, Earthquake Engineering Research Center, University of California, Berkeley, Calif., 1983.
14. Ministry of Communication of the People's Republic of China. *Code for design of highway reinforced concrete bridges and culverts*. China Communications Press, Beijing, 2004.
15. Ma C, Chen WZ. Numerical simulation of coupling time-varying effect of prestress and creep of PC bridge. *Bridge Construction* 2013; **43**(3): 77-82.
16. Mitchell D, Cook WD, Khan AA, Tham T. Influence of high strength concrete on transfer and development length of pretensioning strand. *PCI Journal* 1993; **14**(4): 62-74.
17. Ayoub A, Filippou FC. Finite-element model for pretensioned prestressed concrete girders. *J. Struct.*

Eng. 2010; **136**(4): 401-409.